Verified Hill Region Topology and Parameter Sensitivity in the Sun–Jupiter Restricted Three Body Problem

Mingquan Luo[1], **Yuan Yao**[1] **& Kaiwei Wang**[1]

Received September 3, 2026
Accepted October 16, 2026
Electronic access November 30, 2026

Background and objective: Published studies of the Sun–Jupiter circular restricted three-body problem use slightly different mass parameters and do not all define the Jacobi constant in the same way, which makes their numbers awkward to compare. We ask whether the choice among published mass parameters changes anything qualitative about the Hill regions.
Methods: We collected five mass parameters from the literature and from JPL ephemerides and used interval arithmetic to enclose the collinear equilibria over the whole range they span, with an independent check in exact rational arithmetic. We also corrected a planar Lyapunov orbit near L1 and measured the small-oscillation frequencies near L4.
Results: Over the whole range, the critical Jacobi constants keep the same order, the gaps between them stay above 0.00127185, 0.0365307 and 0.00190647, the collinear points move monotonically with the mass parameter, and the triangular points remain linearly stable. Replacing the older value $\mu = 0.0009537$ by the DE440 value moves L1 by about 3349 km, while the JPL solutions agree with one another to better than a kilometer.
Conclusions: The qualitative picture is the same for every mass parameter in use, and all of these shifts are small compared with the effect of ignoring Jupiter's orbital eccentricity. The orbit and frequencies also serve as reference values for checking numerical codes.

Keywords: circular restricted three body problem; interval arithmetic; DE440; mass parameter sensitivity; periodic orbit verification

Introduction

A Lagrange point is a location where a negligible-mass object can remain stationary relative to two bodies in circular mutual motion. In rotating coordinates, the conserved Jacobi constant limits the speed available at each location, and where the implied squared speed would be negative, motion is impossible. The boundaries of these regions are zero-velocity curves, and the accessible regions they enclose are called Hill regions. As the Jacobi constant decreases, narrow necks open near the collinear Lagrange points. An open neck makes passage energetically possible, although it does not mean that any particular trajectory passes through it[1,2].

The theory is old, but published numbers are not always easy to compare. The Sun–Jupiter mass ratio has been refined as planetary ephemerides and Juno radio tracking have improved[3,4], so papers written at different times use different values. Some authors treat Jupiter alone as the secondary body and others the whole Jovian system, and some add a constant to the Jacobi constant while others do not[2]. When two published tables disagree in the fourth decimal place, it is not always obvious which of these choices is responsible.

Rigorous computer-assisted methods are well established for this problem. They have been used, for example, to prove the existence of heteroclinic connections and of Lyapunov orbits in the Sun–Jupiter system[5,6], and libraries such as CAPD make such proofs practical[7]. Our use of interval arithmetic is much more modest, since it only encloses the roots of a scalar equation. We use it because it allows a single statement covering every published parameter value at once, instead of a separate check for each.

The question addressed here is therefore a narrow one: do the mass parameters found in the literature change the order in which the Hill-region necks open, or the linear stability of the equilibria? We compare five parameter values, record whether each source includes Jupiter's satellites, and certify the result over an interval containing all of them. We also compute two quantities that are useful for testing restricted three-body codes: a planar Lyapunov orbit near L1 and the small-oscillation frequencies near L4. Throughout, we work with the planar circular model.

[1] *American Heritage Schools Palm Beach Campus*

© The National High School Journal of Science 2026

Methods

Model and Conventions

The primary and secondary are placed at $(-\mu,0)$ and $(1-\mu,0)$, with units chosen so that their separation and angular velocity are both one. With gravitational parameters G_1 and G_2, the mass parameter is $\mu = G_2/(G_1+G_2)$. For DE440 we use $G_1 = 132712440041.279419$ km^3 s^{-2} for the Sun and $G_2 = 126712764.100000$ km^3 s^{-2} for the Jovian system, that is, Jupiter together with its satellites[8]. This gives $\mu \approx 0.000953881151935$. Taking the mass ratio from DE440 does not, of course, make the circular model a substitute for the ephemeris itself[3].

Let r_1 and r_2 be the distances to the two primaries. We use the potential and Jacobi constant without an additive shift:

$$\Omega = \frac{x^2+y^2}{2} + \frac{1-\mu}{r_1} + \frac{\mu}{r_2}, \quad C = 2\Omega - v_x^2 - v_y^2. \tag{1}$$

The equations of motion in the rotating frame are

$$\begin{aligned} \frac{dx}{dt} &= v_x, \quad \frac{dy}{dt} = v_y, \\ \frac{dv_x}{dt} &= 2v_y + \Omega_x, \quad \frac{dv_y}{dt} = -2v_x + \Omega_y. \end{aligned} \tag{2}$$

where $r_1^2 = (x+\mu)^2 + y^2$ and $r_2^2 = (x-1+\mu)^2 + y^2$. Some authors, including Koon et al.[2], add $\mu(1-\mu)/2$ to Ω. The resulting shifted constant C_s satisfies

$$C_s = C + \mu(1-\mu), \quad C(L_4) = 3 - \mu(1-\mu), \quad C_s(L_4) = 3. \tag{3}$$

and the same holds at L5. The shift changes the absolute values of the critical constants, but not the positions of the equilibria, their eigenvalues, the gaps between critical constants, or the Hill regions themselves. Before comparing published critical constants, it is therefore necessary to check which convention each source uses. We report both.

Historical Inputs and Interval Design

We use two values from the literature, $\mu = 0.0009537$ (Koon et al. and Wilczak and Zgliczyński[2,5]) and $\mu = 0.00095387536$ (Efthymiopoulos[9]), and three derived from JPL products: the DE405 header, the DE431 mass-parameter kernel and the DE440 table[8,10,11]. The second literature value is close to the DE440 ratio but is not a rounding of it. The exact numerical strings and the passages they come from are listed in Supplementary Note S2. All coordinates and constants in our tables were recomputed from these inputs rather than copied from the original papers.

The interval we certify runs from $\mu = 0.0009537$ up to the DE405 ratio, approximately 0.000953881180363102, which is the largest of the five values. Both endpoints are taken from the exact decimal strings in the sources. The interval simply spans past modeling choices, and its width should not be read as an uncertainty in Jupiter's mass.

The collinear equilibria are the roots of

$$F(x,\mu) = x - \frac{(1-\mu)(x+\mu)}{|x+\mu|^3} - \frac{\mu(x-1+\mu)}{|x-1+\mu|^3} = 0. \tag{4}$$

On each collision-free interval of the x-axis, F is continuous with $F_x = 1 + 2(1-\mu)/r_1^3 + 2\mu/r_2^3 > 0$ and changes sign between the ends of the interval, so L3, L1 and L2 exist and are unique. Supplementary Note S1 gives this standard argument together with the corresponding quintic equations. The triangular points lie at $(1/2-\mu, \pm\sqrt{3}/2)$.

We divided the parameter interval into 256 subintervals and evaluated F in 100-digit decimal arithmetic with outward rounding. For each subinterval M and each collinear point we found a collision-free box $[a,b]$ with $\sup F(a,M) < 0$ and $\inf F(b,M) > 0$, so that the box contains the root for every μ in M. Evaluating the relevant expressions over these boxes then bounds the critical constants and their differences. The derivatives with respect to μ follow from implicit differentiation:

$$\frac{dx_i}{d\mu} = -\frac{F_\mu}{F_x}, \quad \frac{dC_i}{d\mu} = 2\left(\frac{1}{r_2} - \frac{1}{r_1} - x_i\right). \tag{5}$$

The derivatives of the three critical gaps turned out to have a fixed sign over the whole interval, so each gap takes its extreme values at the endpoints. We then tightened the final bounds using separate root enclosures at the two endpoints. As independent checks, we re-evaluated every recorded interval operation in exact rational arithmetic and repeated the computation with 70 digits and 128 subintervals, which gave the same signs. No binary floating-point arithmetic is used in this part of the calculation. The code itself has not been formally verified, so the result is a computer-assisted proof in the usual sense; Note S2 gives the details.

Independent Dynamical Checks

Linearizing about an equilibrium gives the characteristic equation

$$\lambda^4 + (4 - \Omega_{xx} - \Omega_{yy})\lambda^2 + \Omega_{xx}\Omega_{yy} - \Omega_{xy}^2 = 0. \tag{6}$$

At the triangular points the two frequencies satisfy

$$\omega_{s,f}^2 = \frac{1 \mp \sqrt{1 - 27\mu(1-\mu)}}{2}. \tag{7}$$

To test the integration near L4, we started orbits at $x(0) = x_4 + \varepsilon$, $y(0) = y_4$ with zero velocity in the rotating frame, for $\varepsilon = 10^{-5}$, 10^{-4} and 10^{-3}, and integrated each one for 800 time units, or about ten slow periods. Both frequencies were estimated together by a least-squares harmonic fit

© The National High School Journal of Science 2026

to 4001 equally spaced samples, and we checked how much the estimates changed with the number of harmonics and the length of the fitting window. The integrations used DOP853, the explicit eighth-order Dormand–Prince method of Hairer, Nørsett and Wanner [12], and were repeated at tighter tolerances. The periodic orbit was also integrated with the implicit Radau method for comparison. In these floating-point calculations the collinear points were located with Brent's method [13].

Equation (6) is unchanged if both Coriolis terms change sign, so matching frequencies does not show that the frame rotates in the right direction. We therefore also compared the rotating-frame acceleration, transformed to inertial coordinates, with the gravitational acceleration computed directly in the inertial frame, and compared the signed phase of the L4 oscillation with the linear solution.

For the planar Lyapunov orbit near L1, we fixed $x(0) = x_1 - 0.001$ and $y(0) = v_x(0) = 0$ and adjusted $v_y(0)$ by Newton iteration until v_x vanished at the next crossing of $y = 0$, half a period later. The monodromy matrix was obtained by integrating $d\Phi/dt = A(t)\Phi$ with $\Phi(0) = I$ over one full period. Unlike the equilibrium bounds, these orbit results are ordinary floating-point computations. Note S3 lists the event-detection settings, tolerances and fitting details.

Scale and Reproducibility

To express results in kilometers, we use $a_0 = 5.20288700$ au, the J2000 semimajor axis from JPL's approximate planetary elements [14], together with the IAU astronomical unit [15]. This nominal scale is used for illustration only and is independent of the DE440 mass ratio. Dimensionless values are given to enough digits for reproduction, and distances in kilometers are rounded to four significant figures. The study is purely computational and involved no human or animal subjects.

Results

Common-Convention Benchmarks

Table 1 compares L1 for the five inputs. The coordinates and Jacobi constants of all five equilibria in both conventions are given in Note S2 and in the accompanying data file. The two literature sources do not say whether Jupiter's satellites are included, and the table labels them accordingly.

For DE440 the shifted collinear constants are $C_{s1} = 3.039713958548$, $C_{s2} = 3.038441863796$ and $C_{s3} = 3.001906833286$, and $C_s = 3$ exactly at L4 and L5. Without the shift the corresponding values are 3.038760987286, 3.037488892533, 3.000953862024 and 2.999047028737. The offset between the two conventions, about 9.53×10^{-4}, is much larger than any difference between the JPL inputs, so it is the first thing to check when published tables disagree.

Table 1 L1 for the five mass parameters, in barycentric coordinates and the shifted Jacobi convention. All quantities are dimensionless, and μ is multiplied by 10^4. Sources are given in Methods.

Input	$\mu \times 10^4$	x_1	C_{s1}	Secondary
Koon / Wilczak	9.537000000	0.9323697524	3.0397090701	Jupiter; satellites unspecified
Efthymiopoulos	9.538753600	0.9323655873	3.0397138023	Jupiter; satellites unspecified
DE405	9.538811804	0.9323654491	3.0397139593	Jovian system
DE431	9.538811572	0.9323654496	3.0397139587	Jovian system
DE440	9.538811519	0.9323654497	3.0397139585	Jovian system

With the nominal scale held fixed, replacing $\mu = 0.0009537$ by the DE440 value moves L1 by -3349 km and L2 by +3373 km along the x-axis. Replacing the Efthymiopoulos value by DE440 moves them by -107.1 and +107.8 km, and replacing DE405 by DE440 moves them by only +0.5255 and -0.5292 km. These are differences between models at a fixed scale, not predicted changes in the real positions of the Lagrange points.

Parameter-Uniform Result

Proposition. For every μ in the interval defined above, $C_1 > C_2 > C_3 > C_4 = C_5$, $dx_1/d\mu < 0$, $dx_2/d\mu > 0$, $dx_3/d\mu < 0$ and $27\mu(1-\mu) < 1$. The collinear points are saddle–centers and the triangular points are linearly stable. In particular, the Hill-region necks open in the same order for all five parameter values.

Proof. Since $F_x > 0$, each collision-free interval contains exactly one root, and the interval sign conditions enclose it for every μ in each subinterval, including the shared endpoints. Evaluating Equation (5) on these enclosures gives the signs of the derivatives. The positive lower bounds in Table 2 give the order of the critical constants, and its last row gives Routh's condition $27\mu(1-\mu) < 1$. At each collinear point the enclosures give $\Omega_{xx} > 0$ and $\Omega_{yy} < 0$, while $\Omega_{xy} = 0$ by symmetry, so Equation (6), viewed as a quadratic in λ^2, has one positive and one negative root; this is the saddle–center case. $C_4 = C_5$ follows from the symmetry of the triangular points. Since the 256 subintervals cover the whole interval, these conclusions hold for every μ in it. The sequence of Hill regions then follows from the standard description of how the regions change as C passes each critical value, summarized in Note S1. ■

Table 2 Bounds valid over the whole parameter interval, rounded outward.

Quantity	Strict lower bound	Strict upper bound
$C_1 - C_2$	0.00127185	0.00127210
$C_2 - C_3$	0.0365307	0.0365351
$C_3 - C_4$	0.00190647	0.00190684
$27\mu(1-\mu)$	0.02572533	0.025730230

The derivative enclosures are $-23.754 < dx_1/d\mu < -23.750$, $23.918 < dx_2/d\mu < 23.922$ and $-0.416667 < dx_3/d\mu < -0.416666$. Note S1 also shows that $2\Omega \geq C_4$ everywhere, with equality only at L4 and L5. Table 3 lists the six regimes of the Hill region as C decreases, and Figure 1 shows each of them. In panels (a)–(d) we used values of C between the critical levels so that the necks have visible width.

Table 3 Changes in the Hill region as C decreases. At C_1, C_2 and C_3 the corresponding neck has zero width. Collision points are excluded throughout.

Range	Geometric change	Figure 1
$C > C_1$	Three allowed components; both primary lobes isolated from exterior.	(a)
$C_2 < C < C_1$	L1 neck connects primary lobes; exterior remains separate.	(b)
$C_3 < C < C_2$	L2 neck connects the interior to exterior.	(c)
$C_4 < C < C_3$	L3 passage also opens; two forbidden regions remain.	(d)
$C = C_4 = C_5$	No forbidden area; zero-velocity locus reduces to L4 and L5.	(e)
$C < C_4$	Entire collision-free plane allowed; zero-velocity locus empty.	(f)

Orbit and Frequency Verification

The corrected L1 orbit starts at $(x, y, v_x, v_y) = (0.931365449731, 0, 0, 0.00742833322210)$ and has period 2.88599403264 and Jacobi constant $C = 3.038715607033$. Five Newton iterations reduced the closure error after one period below 2×10^{-13} in the Euclidean norm of the state, and the Radau trajectory agrees with the DOP853 one to within 4×10^{-12}. The monodromy matrix has the hyperbolic pair of multipliers 2283.76525 and 0.000437873375, and the remaining two multipliers equal one to numerical precision, as expected for a periodic orbit of an autonomous Hamiltonian system. The product of the hyperbolic pair differs from one by less than 5×10^{-10} and the symplectic residual is below 2×10^{-9}, so only the leading digits of the multipliers are reliable. Closure was computed from the unrounded initial state given in the data file, and Figure S2 compares results at different tolerances.

At L4, Equation (7) gives $\omega_s = 0.0804641214931$ and $\omega_f = 0.996757505692$, corresponding to periods 78.08679434 and 6.303624775. For $\varepsilon = 10^{-5}$ the fitted frequencies differ from these values by 2.60×10^{-8} and 2.93×10^{-10} in relative terms. Each tenfold increase in ε makes these differences about a hundred times larger (Figure 2c). This quadratic dependence on amplitude is what the leading nonlinear terms predict[16], so the differences reflect the dynamics rather than integration error.

In the sign test, the correct equations reproduce the inertial acceleration to within 4.5×10^{-16} at the sampled points, whereas reversing both Coriolis terms produces errors larger than 0.083. The signed phase comparison also rejects the reversed equations. Neither Jacobi conservation nor the frequencies alone would have revealed this kind of error.

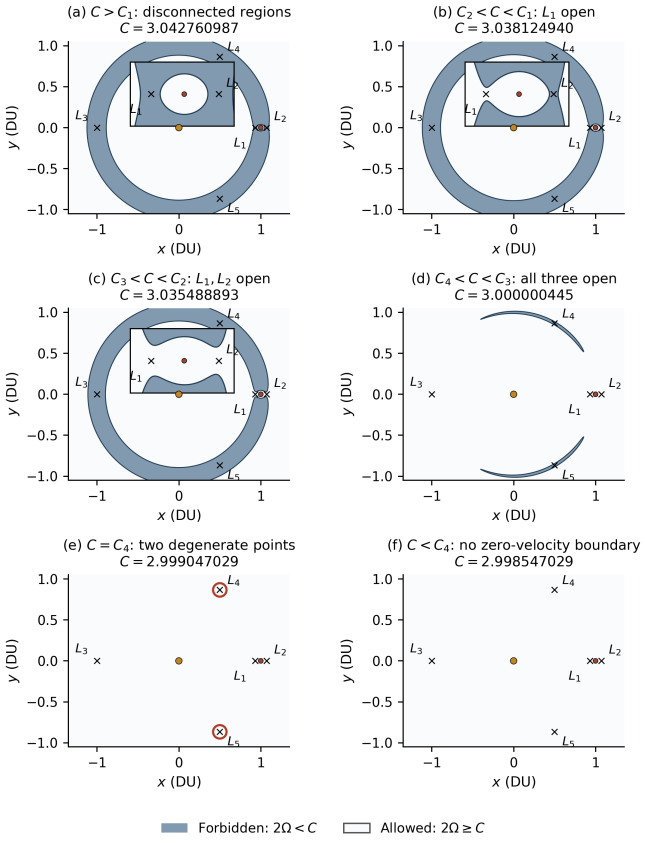


Figure. 1 Hill regions of the Sun–Jupiter system (DE440) as C decreases. Shaded areas are forbidden ($2\Omega < C$), and the panel titles give the shifted constant C_s. The insets in (a)–(c) show the neighborhood of Jupiter at a larger scale. Panels (a)–(d) use values of C between critical levels. In (e), $C = C_4$ and the forbidden region shrinks to the points L4 and L5; in (f) there is no forbidden region. Distances are in normalized units (DU).

Discussion

The equilibria, Routh's criterion and the sequence of Hill regions are textbook material[1]. What this paper adds is a check, with explicit bounds, that the qualitative picture is the same for every mass parameter used in the Sun–Jupiter literature, together with a set of reference values for testing code. The rigorous studies cited in the Introduction answer much harder

© The National High School Journal of Science 2026

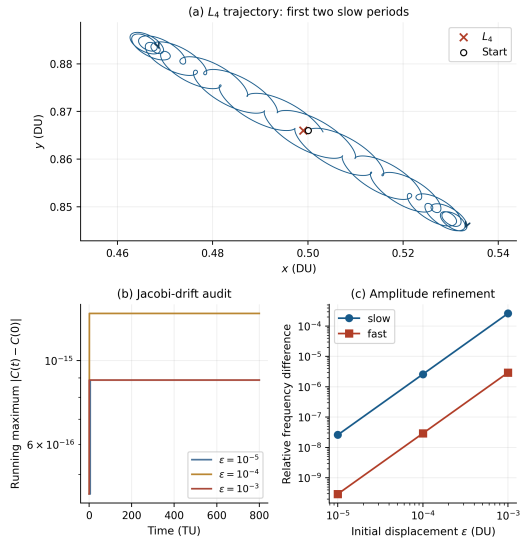


Figure. 2 Small oscillations about L4. (a) The first two slow periods for $\varepsilon = 10^{-3}$. (b) Running maximum of the error in the Jacobi constant over 800 time units; it remains at the level of double-precision rounding with no visible growth. (c) Relative difference between the fitted and linear frequencies as a function of ε. The slope of about 2 indicates a quadratic dependence on amplitude.

questions about orbits and transport, which we do not address here.

For the planar problem, nonlinear stability of the triangular points is already known. Deprit and Deprit-Bartholomé [17] proved Lyapunov stability for all μ below the Routh value except at three special values, approximately 0.024293, 0.013516 and 0.010914, where their criterion does not decide the question. All five Sun–Jupiter values lie far from these, so their theorem applies to every case studied here. Our integrations are consistent with this result, but since they cover a finite time they do not prove it, and they say nothing about the spatial problem or the real Solar System.

The main physical limitation is the assumption of a circular orbit. With Jupiter's eccentricity $e = 0.04838624$ from the same element set, the Sun–Jupiter distance varies by $\pm a_0 e \approx \pm 3.766 \times 10^7$ km. Scaling the distance from Jupiter to L1 by the same factor gives about $\pm 2.511 \times 10^6$ km. This is only a rough indication, because the elliptic problem is time-dependent and allows behavior, such as global instability, that the circular model cannot show [18]. Even so, it is several orders of magnitude larger than the differences between mass parameters in Table 1, which are in turn much larger than the numerical error in the computed roots.

The frequency estimates depend slightly on the fitting window, the number of harmonics and the amplitude, and Note S3 reports the size of these variations. The figures are illustrations only, and the statements about the Hill regions rest on the proposition rather than on the plotted contours.

Conclusion

For all five Sun–Jupiter mass parameters considered, the critical Jacobi constants occur in the same order, the gaps between them are bounded well away from zero, and the equilibria have the same stability type. When published values disagree, the Jacobi convention should be checked first, because its offset of about 9.53×10^{-4} is larger than the effect of any of the mass-parameter changes. The JPL solutions themselves agree to well under a kilometer in the position of L1. The L1 orbit, the L4 frequencies and the Coriolis sign test give simple benchmarks for checking restricted three-body codes. A natural extension is the elliptic problem, where Jupiter's eccentricity outweighs all of the effects considered here.

Data and Code Availability

The Supporting Information contains Notes S1–S3, the analysis code, the interval certificates and their rational re-evaluation, the numerical tables and figures, snapshots of the JPL source files with checksums, and instructions for reproducing the results. This work received no external funding.

References

1 V. Szebehely. Theory of orbits: the restricted problem of three bodies. Academic Press, 1967, https://doi.org/10.1016/B978-0-12-395732-0.X5001-6.

2 W. S. Koon, M. W. Lo, J. E. Marsden, S. D. Ross. Heteroclinic connections between periodic orbits and resonance transitions in celestial mechanics. Chaos: An Interdisciplinary Journal of Nonlinear Science. Vol. 10, pg. 427–469, 2000, https://doi.org/10.1063/1.166509.

3 R. S. Park, W. M. Folkner, J. G. Williams, D. H. Boggs. The JPL planetary and lunar ephemerides DE440 and DE441. The Astronomical Journal. Vol. 161, pg. 105, 2021, https://doi.org/10.3847/1538-3881/abd414.

4 V. Notaro, D. Durante, L. Iess, S. J. Bolton. Determination of Jupiter's mass from Juno radio tracking data. Journal of Guidance, Control, and Dynamics. Vol. 44, pg. 1062–1067, 2021, https://doi.org/10.2514/1.g005311.

5 D. Wilczak, P. Zgliczyński. Heteroclinic connections between periodic orbits in planar restricted circular three-body problem - a computer assisted proof. Communications in Mathematical Physics. Vol. 234, pg. 37–75, 2003, https://doi.org/10.1007/s00220-002-0709-0.

6 M. J. Capiński. Computer assisted existence proofs of Lyapunov orbits at L2 and transversal intersections of invariant manifolds in the Jupiter–Sun PCR3BP. SIAM Journal on Applied Dynamical Systems. Vol. 11, pg. 1723–1753, 2012, https://doi.org/10.1137/110847366.

7 T. Kapela, M. Mrozek, D. Wilczak, P. Zgliczyński. CAPD::DynSys: a flexible C++ toolbox for rigorous numerical analysis of dynamical systems. Communications in Nonlinear Science and Numerical Simulation. Vol. 101, pg. 105578, 2021, https://doi.org/10.1016/j.cnsns.2020.105578.

8 NASA Jet Propulsion Laboratory. Astrodynamic parameters, DE440 planetary-system gravitational parameters. https://ssd.jpl.nasa

.gov/astro_par.html, n.d. Accessed 16 September 2026; source snapshot in Supporting Information.
9 C. Efthymiopoulos. Nekhoroshev stability estimates for different models of the Trojan asteroids. Proceedings of the International Astronomical Union. Vol. 2004(IAUC197), pg. 195–204, 2004, https://doi.org/10.1017/s1743921304008658.
10 NASA Jet Propulsion Laboratory. DE405 ASCII ephemeris header, header.405, groups 1040 and 1041. https://ssd.jpl.nasa.gov/ftp/eph/planets/ascii/de405/header.405, n.d. Accessed 16 September 2026.
11 NASA Jet Propulsion Laboratory. DE431 mass-parameter kernel, gm_de431.tpc. https://naif.jpl.nasa.gov/pub/naif/generic_kernels/pck/gm_de431.tpc, 2014. Last modified 8 January 2014; accessed 16 September 2026.
12 E. Hairer, S. P. Nørsett, G. Wanner. Solving ordinary differential equations I: nonstiff problems. 2nd ed. Springer, 1993, https://doi.org/10.1007/978-3-540-78862-1.
13 R. P. Brent. An algorithm with guaranteed convergence for finding a zero of a function. The Computer Journal. Vol. 14, pg. 422–425, 1971, https://doi.org/10.1093/comjnl/14.4.422.
14 NASA Jet Propulsion Laboratory. Approximate positions of the planets, 1800–2050 element fit and nominal errors. https://ssd.jpl.nasa.gov/planets/approx_pos.html, n.d. Accessed 16 September 2026; source snapshot in Supporting Information.
15 International Astronomical Union. Resolution B2 on the re-definition of the astronomical unit of length. XXVIII General Assembly, 2012, https://iauarchive.eso.org/static/resolutions/IAU2012_English.pdf.
16 R. I. Páez, U. Locatelli, C. Efthymiopoulos. New Hamiltonian expansions adapted to the Trojan problem. Celestial Mechanics and Dynamical Astronomy. Vol. 126, pg. 519–541, 2016, https://doi.org/10.1007/s10569-016-9710-3.
17 A. Deprit, A. Deprit-Bartholomé. Stability of the triangular Lagrangian points. The Astronomical Journal. Vol. 72, pg. 173–179, 1967, https://doi.org/10.1086/110213.
18 A. Delshams, V. Kaloshin, A. de la Rosa, T. M. Seara. Global instability in the restricted planar elliptic three body problem. Communications in Mathematical Physics. Vol. 366, pg. 1173–1228, 2019, https://doi.org/10.1007/s00220-018-3248-z.

Supplementary information

The online version contains supplementary material available at https://nhsjs.com/?p=62576

© The National High School Journal of Science 2026